

Cosmological Constraints from Full-Scale Clustering and Galaxy–Galaxy Lensing with DESI DR1

J. U. LANGE,¹ A. WELLS,² A. HEARIN,³ G. BELTZ-MOHRMANN,⁴ A. LEAUTAUD,^{5,6} S. HEYDENREICH,⁵ C. BLAKE,⁷ J. AGUILAR,⁸ S. AHLEN,⁹ A. ANAND,⁸ D. BIANCHI,^{10,11} D. BROOKS,¹² F. J. CASTANDER,^{13,14} T. CLAYBAUGH,⁸ S. COLE,¹⁵ A. CUCEU,⁸ K. S. DAWSON,¹⁶ A. DE LA MACORRA,¹⁷ BIPRATEEP DEY,^{18,19} P. DOEL,¹² A. ELLIOTT,^{20,21} N. EMAS,⁷ S. FERRARO,^{8,22} A. FONT-RIBERA,²³ J. E. FORERO-ROMERO,^{24,25} C. GARCIA-QUINTERO,²⁶ E. GAZTAÑAGA,^{13,27,14} S. GONTCHO A GONTCHO,^{8,28} G. GUTIERREZ,²⁹ J. GUY,⁸ K. HONSCHIED,^{30,20,21} D. HUTERER,^{31,32} M. ISHAK,³³ S. JOURDAK,³⁴ R. JOYCE,³⁵ R. KEHOE,³⁶ D. KIRKBY,³⁷ T. KISNER,⁸ A. KREMIN,⁸ A. KROLEWSKI,^{38,39,40} O. LAHAV,¹² C. LAMMAN,²¹ M. LANDRIAUX,⁸ L. LE GUILLOU,⁴¹ M. E. LEVI,⁸ M. MANERA,^{42,23} P. MARTINI,^{30,43,21} A. MEISNER,³⁵ R. MIQUEL,^{44,23} J. MOUSTAKAS,⁴⁵ E. MUELLELR,⁴⁶ S. NADATHUR,²⁷ J. A. NEWMAN,¹⁹ G. NIZ,^{47,48} N. PALANQUE-DELABROUILLE,^{49,8} W. J. PERCIVAL,^{38,39,40} C. POPPETT,^{8,50,22} A. PORREDON,^{34,51,52,21} F. PRADA,⁵³ I. PÉREZ-RÀFOLS,⁵⁴ A. ROBERTSON,³⁵ G. ROSSI,⁵⁵ R. RUGGERI,⁵⁶ E. SANCHEZ,³⁴ C. SAULDER,⁵⁷ D. SCHLEGEL,⁸ M. SCHUBNELL,^{31,32} A. SEMENAITE,⁷ H. SEO,² J. SILBER,⁸ D. SPRAYBERRY,³⁵ Z. SUN,⁵⁸ G. TARLÉ,³² M. VARGAS-MAGAÑA,¹⁷ B. A. WEAVER,³⁵ R. H. WECHSLER,^{59,60,61} P. ZARROUK,⁴¹ R. ZHOU,⁸ AND H. ZOU⁶²

¹Department of Physics, American University, 4400 Massachusetts Avenue NW, Washington, DC 20016, USA

²Department of Physics & Astronomy, Ohio University, 139 University Terrace, Athens, OH 45701, USA

³Argonne National Laboratory, High-Energy Physics Division, 9700 S. Cass Avenue, Argonne, IL 60439, USA

⁴Department of Physics, Smith College, 1 Chapin Way, Northampton, MA 01063, USA

⁵Department of Astronomy and Astrophysics, UCO/Lick Observatory, University of California, 1156 High Street, Santa Cruz, CA 95064, USA

⁶Department of Astronomy and Astrophysics, University of California, Santa Cruz, 1156 High Street, Santa Cruz, CA 95065, USA

⁷Centre for Astrophysics & Supercomputing, Swinburne University of Technology, P.O. Box 218, Hawthorn, VIC 3122, Australia

⁸Lawrence Berkeley National Laboratory, 1 Cyclotron Road, Berkeley, CA 94720, USA

⁹Department of Physics, Boston University, 590 Commonwealth Avenue, Boston, MA 02215 USA

¹⁰Dipartimento di Fisica “Aldo Pontremoli”, Università degli Studi di Milano, Via Celoria 16, I-20133 Milano, Italy

¹¹INAF-Osservatorio Astronomico di Brera, Via Brera 28, 20122 Milano, Italy

¹²Department of Physics & Astronomy, University College London, Gower Street, London, WC1E 6BT, UK

¹³Institut d’Estudis Espacials de Catalunya (IEEC), c/ Esteve Terradas 1, Edifici RDIT, Campus PMT-UPC, 08860 Castelldefels, Spain

¹⁴Institute of Space Sciences, ICE-CSIC, Campus UAB, Carrer de Can Magrans s/n, 08913 Bellaterra, Barcelona, Spain

¹⁵Institute for Computational Cosmology, Department of Physics, Durham University, South Road, Durham DH1 3LE, UK

¹⁶Department of Physics and Astronomy, The University of Utah, 115 South 1400 East, Salt Lake City, UT 84112, USA

¹⁷Instituto de Física, Universidad Nacional Autónoma de México, Circuito de la Investigación Científica, Ciudad Universitaria, Cd. de México C. P. 04510, México

¹⁸Department of Astronomy & Astrophysics, University of Toronto, Toronto, ON M5S 3H4, Canada

¹⁹Department of Physics & Astronomy and Pittsburgh Particle Physics, Astrophysics, and Cosmology Center (PITT PACC), University of Pittsburgh, 3941 O’Hara Street, Pittsburgh, PA 15260, USA

²⁰Department of Physics, The Ohio State University, 191 West Woodruff Avenue, Columbus, OH 43210, USA

²¹The Ohio State University, Columbus, 43210 OH, USA

²²University of California, Berkeley, 110 Sproul Hall #5800 Berkeley, CA 94720, USA

²³Institut de Física d’Altes Energies (IFAE), The Barcelona Institute of Science and Technology, Edifici Cn, Campus UAB, 08193, Bellaterra (Barcelona), Spain

²⁴Departamento de Física, Universidad de los Andes, Cra. 1 No. 18A-10, Edificio Ip, CP 111711, Bogotá, Colombia

²⁵Observatorio Astronómico, Universidad de los Andes, Cra. 1 No. 18A-10, Edificio H, CP 111711 Bogotá, Colombia

²⁶Center for Astrophysics | Harvard & Smithsonian, 60 Garden Street, Cambridge, MA 02138, USA

²⁷Institute of Cosmology and Gravitation, University of Portsmouth, Dennis Sciama Building, Portsmouth, PO1 3FX, UK

²⁸University of Virginia, Department of Astronomy, Charlottesville, VA 22904, USA

²⁹Fermi National Accelerator Laboratory, PO Box 500, Batavia, IL 60510, USA

³⁰Center for Cosmology and AstroParticle Physics, The Ohio State University, 191 West Woodruff Avenue, Columbus, OH 43210, USA

³¹Department of Physics, University of Michigan, 450 Church Street, Ann Arbor, MI 48109, USA

³²University of Michigan, 500 S. State Street, Ann Arbor, MI 48109, USA

³³Department of Physics, The University of Texas at Dallas, 800 W. Campbell Rd., Richardson, TX 75080, USA

³⁴CIEMAT, Avenida Complutense 40, E-28040 Madrid, Spain

³⁵NSF NOIRLab, 950 N. Cherry Ave., Tucson, AZ 85719, USA

³⁶Department of Physics, Southern Methodist University, 3215 Daniel Avenue, Dallas, TX 75275, USA

³⁷Department of Physics and Astronomy, University of California, Irvine, 92697, USA

³⁸Department of Physics and Astronomy, University of Waterloo, 200 University Ave W, Waterloo, ON N2L 3G1, Canada

³⁹Perimeter Institute for Theoretical Physics, 31 Caroline St. North, Waterloo, ON N2L 2Y5, Canada

⁴⁰Waterloo Centre for Astrophysics, University of Waterloo, 200 University Ave W, Waterloo, ON N2L 3G1, Canada

⁴¹Sorbonne Université, CNRS/IN2P3, Laboratoire de Physique Nucléaire et de Hautes Energies (LPNHE), FR-75005 Paris, France

⁴²Departament de Física, Serra Húnter, Universitat Autònoma de Barcelona, 08193 Bellaterra (Barcelona), Spain

⁴³Department of Astronomy, The Ohio State University, 4055 McPherson Laboratory, 140 W 18th Avenue, Columbus, OH 43210, USA

⁴⁴Institució Catalana de Recerca i Estudis Avançats, Passeig de Lluís Companys, 23, 08010 Barcelona, Spain

⁴⁵Department of Physics and Astronomy, Siena University, 515 Loudon Road, Loudonville, NY 12211, USA

⁴⁶Department of Physics and Astronomy, University of Sussex, Brighton BN1 9QH, U.K

⁴⁷Departamento de Física, DCI-Campus León, Universidad de Guanajuato, Loma del Bosque 103, León, Guanajuato C. P. 37150, México

⁴⁸Instituto Avanzado de Cosmología A. C., San Marcos 11 - Atenas 202. Magdalena Contreras. Ciudad de México C. P. 10720, México

⁴⁹IRFU, CEA, Université Paris-Saclay, F-91191 Gif-sur-Yvette, France

⁵⁰Space Sciences Laboratory, University of California, Berkeley, 7 Gauss Way, Berkeley, CA 94720, USA

⁵¹Institute for Astronomy, University of Edinburgh, Royal Observatory, Blackford Hill, Edinburgh EH9 3HJ, UK

⁵²Ruhr University Bochum, Faculty of Physics and Astronomy, Astronomical Institute (AIRUB), German Centre for Cosmological Lensing, 44780 Bochum, Germany

⁵³Instituto de Astrofísica de Andalucía (CSIC), Glorieta de la Astronomía, s/n, E-18008 Granada, Spain

⁵⁴Departament de Física, EEBE, Universitat Politècnica de Catalunya, c/Eduard Maristany 10, 08930 Barcelona, Spain

⁵⁵Department of Physics and Astronomy, Sejong University, 209 Neungdong-ro, Gwangjin-gu, Seoul 05006, Republic of Korea

⁵⁶Queensland University of Technology, School of Chemistry & Physics, George St, Brisbane 4001, Australia

⁵⁷Max Planck Institute for Extraterrestrial Physics, Gießenbachstraße 1, 85748 Garching, Germany

⁵⁸Department of Astronomy, Tsinghua University, 30 Shuangqing Road, Haidian District, Beijing, China, 100190

⁵⁹Kavli Institute for Particle Astrophysics and Cosmology, Stanford University, Menlo Park, CA 94305, USA

⁶⁰Physics Department, Stanford University, Stanford, CA 93405, USA

⁶¹SLAC National Accelerator Laboratory, 2575 Sand Hill Road, Menlo Park, CA 94025, USA

⁶²National Astronomical Observatories, Chinese Academy of Sciences, A20 Datun Road, Chaoyang District, Beijing, 100101, P. R. China

ABSTRACT

We present constraints on cosmic structure growth from the analysis of galaxy clustering and galaxy-galaxy lensing with galaxies from the Dark Energy Spectroscopic Instrument (DESI) Data Release 1. We analyze four samples drawn from the Bright Galaxy Survey (BGS) and the Luminous Red Galaxy (LRG) target classes. Projected galaxy clustering measurements from DESI are supplemented with lensing measurements from the Dark Energy Survey (DES), the Kilo-Degree Survey (KiDS), and the Hyper Suprime-Cam (HSC) survey around the same targets. Our method relies on a simulation-based modeling framework using the AbacusSummit simulations and a complex halo occupation distribution model that incorporates assembly bias. We analyze scales down to $0.4 h^{-1}$ Mpc for clustering and $2.5 h^{-1}$ Mpc for lensing, leading to stringent constraints on $S_8 = \sigma_8 \sqrt{\Omega_m/0.3}$ and Ω_m when fixing other cosmological parameters to those preferred by the CMB. We find $S_8 = 0.794 \pm 0.023$ and $\Omega_m = 0.295 \pm 0.012$ when using lensing measurements from DES and KiDS. Similarly, for HSC, we find $S_8 = 0.793 \pm 0.017$ and $\Omega_m = 0.303 \pm 0.010$ when assuming the best-fit photometric redshift offset suggested by the HSC collaboration. Overall, our results are in good agreement with other results in the literature while continuing to highlight the constraining power of non-linear scales.

Keywords: Redshift surveys(1378), Weak gravitational lensing(1797), Astrostatistics (1882)

1. INTRODUCTION

The advent of large galaxy surveys such as the Dark Energy Spectroscopic Instrument (DESI; Levi et al.

2013; DESI Collaboration et al. 2016a,b, 2022; Silber et al. 2023; Guy et al. 2023; Schlaflay et al. 2023; Miller et al. 2024; Poppett et al. 2024; DESI Collaboration

et al. 2024a,b, 2025), the Dark Energy Survey (DES; Flaugher et al. 2015; Abbott et al. 2022), the Subaru Hyper Suprime-Cam Survey (HSC; Aihara et al. 2018; More et al. 2023), and the Kilo-Degree Survey (KiDS; Kuijken et al. 2015; Asgari et al. 2021) has ushered in a new era in precision measurements of the large-scale structure of the Universe. These new measurements of matter and galaxy distributions have delivered important insights into the properties dark energy and gravity as well as tests of our cosmological models (see, e.g., Abbott et al. 2022; Sugiyama et al. 2023; Ishak et al. 2025; Adame et al. 2025a; Abdul Karim et al. 2025; Wright et al. 2025). Alongside the advance in data quality and quantity, there has been significant effort to develop new analysis methods that can extract more cosmological information from existing data.

One promising avenue to maximize information is to extend the analysis of the galaxy and matter distribution to so-called non-linear scales, i.e., scales smaller than $\mathcal{O}(10 h^{-1} \text{Mpc})$. Interpreting non-linear scales is challenging due to non-linear gravitational effects, the complex relationship between galaxies and dark matter halos (Wechsler & Tinker 2018), and the impact of baryonic physics on the matter distribution (see, e.g., van Daalen et al. 2011; Springel et al. 2018; van Daalen et al. 2020). However, recent studies have shown how to address these issues through advancements in cosmological simulations and machine learning (see, e.g., Yuan et al. 2022; Zhai et al. 2023; Miyatake et al. 2023; Hahn et al. 2023a; Lange et al. 2023, for recent applications). Other promising directions are the analysis of higher-order clustering (see, e.g., Hahn & Villaescusa-Navarro 2021; Valogiannis et al. 2024; Liu et al. 2025), including field-level inference (see, e.g., Nguyen et al. 2024) and more physically-motivated priors on bias parameters (see, e.g. Ivanov et al. 2025).

In this work, we focus on the combined analysis of galaxy clustering and weak gravitational lensing. The clustering of galaxy is measured with data from DESI Data Release 1. We supplement these clustering measurements with lensing measurements from the latest publicly available lensing data from DES, KiDS, and HSC. Such an analysis, sometimes called a “2×2pt” analysis, places constraints on $S_8 = \sigma_8 \sqrt{\Omega_m/0.3}$, where σ_8 is the root mean square of matter fluctuations on a scale of $8 h^{-1} \text{Mpc}$ and Ω_m is the matter density. The present analysis focuses on analyzing non-linear scales using advanced simulation-based modeling. It is complementary to another study by Porredon et al. (in prep.) that analyzes the matter and galaxy distribution on larger scales and also includes cosmic shear data in a so-called “3×2pt” analysis.

Our analysis provides new insights into the so-called S_8 -tension, a possible discrepancy between inferred values of S_8 between studies of the Cosmic Microwave Background (CMB) and low-redshift probes such as gravitational lensing (Abdalla et al. 2022). Early work by Cacciato et al. (2013), who studied lensing and clustering down to small scales, found values for S_8 significantly below than that preferred by the Planck Collaboration et al. (2020) CMB analysis, $S_8 = 0.825 \pm 0.011$. Whereas the analysis by Cacciato et al. (2013) was based on an analytic halo model, many recent studies employ simulation-based modeling to predict galaxy clustering and lensing. One such example is the study by Leauthaud et al. (2017) that showed that the lensing amplitude at fixed clustering is significantly overpredicted when one assumes cosmological parameters preferred by CMB studies. However, this discrepancy may also be related to galaxy physics such as baryonic feedback and galaxy assembly bias (Leauthaud et al. 2017; Lange et al. 2019b; Amon & Efstathiou 2022; Chaves-Montero et al. 2023). Subsequent studies mitigated the impact of unknown galaxy physics through scale cuts but generally continued to find low values for S_8 . For example, Miyatake et al. (2023), analyzing HSC data together with clustering measurements from the Baryon Oscillation Spectroscopic Survey (BOSS; Reid et al. 2016; Ahumada et al. 2020) found $S_8 = 0.763^{+0.040}_{-0.036}$. Similarly, the analysis of BOSS clustering and DES and KiDS lensing by Lange et al. (2023) yielded $S_8 = 0.792 \pm 0.022$ (also see Wibking et al. 2020; Dvornik et al. 2023; Amon et al. 2023). In this work, we build upon these studies using new measurements from DESI, the successor to BOSS.

We begin by outlining our data and measurements in section 2. Next, we describe our analysis method, including tests on simulated mock catalogs, in section 3. Our main results are presented in section 4 before discussing and summarizing our findings in section 5.

2. MEASUREMENTS

Our analysis relies on galaxy clustering measurements from DESI Data Release 1, supplemented with gravitational lensing measurements from DES Year 3 (DES Y3; Gatti et al. 2021), the KiDS Data Release 4 (KiDS-1000; Giblin et al. 2021), and HSC Year 3 (HSC Y3; Li et al. 2022) data. The measurements are described in detail in Heydenreich et al. (2025) and we summarize the most salient points here. All measurements assume $\Omega_m = 0.3075$ (Planck Collaboration et al. 2016) to convert redshifts and angles into physical coordinates.

2.1. DESI Samples

The different galaxy samples were investigated in [Yuan et al. \(2024\)](#) and balance increased number density with the need for negligible redshift evolution within each sample. DESI targets different classes of extragalactic objects. Those at lower redshift, $z < 1$, i.e., those for which we can get precise galaxy–galaxy lensing measurements, are the Bright Galaxy Survey (BGS) and the Luminous Red Galaxy (LRG) sample.

The BGS Bright targets include all objects with an apparent r -band magnitude brighter than 19.5 ([Hahn et al. 2023b](#)) and covers an area of around $7,500 \text{ deg}^2$ ([Adame et al. 2025b](#)). Due to being a flux-limited survey, the BGS includes many low-redshift targets with a strongly redshift-dependent number density. As a result, we need to apply additional cuts on the absolute k-corrected and evolution-corrected magnitudes M_r ([Moustakas et al. 2023](#); [DESI Collaboration et al. 2024b](#)). We have three BGS samples, BGS1, BGS2, and BGS3. Their redshift ranges are defined by the boundaries [0.1, 0.2, 0.3, 0.4] and the absolute luminosity thresholds are $M_r < -19.5$, -20.5 , and -21 , respectively. However, we do not use BGS1 in our analysis since our simulations do not have sufficient mass resolution to model this low-luminosity sample. In particular, the number density of BGS1 significantly exceeds the number of resolved halos in the simulation. Since the number density of central galaxies cannot exceed that of resolved halos, this forces a very high satellite fraction in the fit and an overall unacceptable χ^2 . A set of higher-resolution simulations would be needed to effectively model this sample.

The LRG sample has a slightly more complicated selection based on the g , r , z , and $W1$ magnitudes ([Zhou et al. 2023](#)) and covers an area of around $5,700 \text{ deg}^2$. Fortunately, the LRG selection does not result in a strongly redshift-dependent number density. Thus, we define three LRG samples, LRG1, LRG2, and LRG3, by the redshift boundaries [0.4, 0.6, 0.8, 1.1]. However, for our main analysis, we do not use LRG3 since these measurements are potentially strongly contaminated by intrinsic alignments, lens magnification and other lensing systematics ([Heydenreich et al. 2025](#)).

For all samples, we use the galaxy number density n_{gal} as a constraint. The number density, like the clustering measurements described below, do correct for incompleteness in the DESI fiber assignment using weights. Uncertainties are derived from jackknife resampling. The number densities are $(3.71 \pm 0.03) \times 10^{-3}$, $(1.38 \pm 0.01) \times 10^{-3}$, $(5.70 \pm 0.03) \times 10^{-4}$, and $(5.69 \pm 0.03) \times 10^{-4} h^3 \text{ Mpc}^{-3}$ for BGS2, BGS3, LRG1, and LRG2, respectively.

2.2. Galaxy Clustering

Galaxy clustering is measured via the projected two-point correlation function w_p ,

$$w_p(r_p) = 2 \int_0^{\pi_{\max}} \xi(r_p, r_\pi) dr_\pi. \quad (1)$$

In the above equation, $\xi(r_p, r_\pi)$ denotes the redshift-space two-point correlation function as a function of the perpendicular, r_p , and line-of-sight direction, r_π . By integrating along the line-of-sight direction out to $\pi_{\max} = 80 h^{-1} \text{ Mpc}$ we reduce sensitivity to redshift-space distortions. The clustering measurements are corrected for fiber incompleteness via pairwise-inverse-probability (PIP) weights and angular upweighting ([Bianchi et al. 2018, 2025](#)).

We measure w_p in 14 logarithmic, comoving r_p bins going from $10^{-1} h^{-1} \text{ Mpc}$ to $10^{1.8} h^{-1} \text{ Mpc}$ but only use data above $0.4 h^{-1} \text{ Mpc}$ for our analysis. Uncertainties are estimated from jackknife resampling with 128 equal-area patches on the sky. Finally, for the inverse of the covariance matrix, we use the Hartlap correction factor ([Hartlap et al. 2007](#)).

2.3. Gravitational Lensing

We also measure the galaxy–galaxy lensing signal around DESI samples to probe the mass distribution around them. Galaxy shape measurements come from the publicly available DES, KiDS, and HSC catalogs. The DES weak lensing catalogs are based on the 3-year data set, utilize four tomographic bins based on r_{iz} colors, have an effective number density of 6 arcmin^{-2} , and span an area of around $4,100 \text{ deg}^2$. KiDS uses a more extensive nine-band photometry to define its five tomographic bins and has a similar number density over a smaller 800 deg^2 area. Given its area, it is called the KiDS-1000 data set. Finally, the HSC year-3 data is significantly deeper with a number density of 15 arcmin^{-2} , four tomographic bins derived from five optical bands, but a much smaller 400 deg^2 area.

The galaxy–galaxy lensing amplitude is a measure of the so-called excess surface density $\Delta\Sigma$ around DESI galaxies,

$$\Delta\Sigma(r_p) = \frac{2}{r_p^2} \int_0^{r_p} \hat{r}_p \Sigma(\hat{r}_p) d\hat{r}_p - \Sigma(r_p), \quad (2)$$

where $\Sigma(r_p)$ is the projected mass density at a certain distance r_p perpendicular to the line of sight. In practice, $\Delta\Sigma$ is inferred from the mean tangential shear γ_t ,

$$\gamma_t(r_p) = \frac{\Delta\Sigma(r_p)}{\Sigma_{\text{crit}}(z_l, z_s)} \quad (3)$$

of “source” galaxies in DES Y3, KiDS-1000, and HSC Y3 around DESI “lens” galaxies. In the above equation, Σ_{crit} is the critical surface density and depends on both the lens, z_l , and the source redshift, z_s . We refer the reader to Heydenreich et al. (2025) for a detailed discussion of how these measurements are performed. We use the lensing measurements employing the conservative lens-source cuts, as outlined in Table 1 of Heydenreich et al. (2025). These lens-source cuts require that at most 3% of sources are at the redshift of the DESI lenses. Employing such cuts reduces systematic uncertainties related to, among others, intrinsic alignments and boost factors (Lange et al. 2024). This implies that we do not use DES and KiDS lensing measurements for LRG2. We correct for lens magnification (Unruh et al. 2020) assuming the best-fit Planck Collaboration et al. (2020) cosmological parameters. Since lens magnification is a small, $\lesssim 10\%$ effect, we neglect its cosmological dependence. We also do not explicitly correct for intrinsic alignment contamination since the effect is expected to be small, i.e., at the level of 1% (Lange et al. 2024). However, there is substantial uncertainty on the magnitude of intrinsic alignments and future studies using higher-precision lensing measurements should investigate potential corrections.

We measure $\Delta\Sigma$ in 13 logarithmic, comoving bins going from $10^{-1} h^{-1} \text{Mpc}$ to $10^{1.6} h^{-1} \text{Mpc}$. To avoid sensitivity to baryonic effects and subhalo lensing (see, e.g., Zu & Mandelbaum 2015; Lange et al. 2019b; Amodeo et al. 2021), we only use scales larger than $2.5 h^{-1} \text{Mpc}$ for our analysis. While baryonic effects will also impact the distribution of satellite galaxies and thereby clustering, we marginalize over this in our analysis. This is why we employ a lower minimum scale for clustering than lensing. We estimate uncertainties using the same jackknife procedure as for clustering. We ignore possible correlations between clustering and lensing amplitudes. Those are expected to be small given that clustering is measured over the full DESI footprint whereas the lensing amplitude measurements are limited to the overlap area with the lensing surveys.

For our cosmological analysis, we combine lensing measurements made for the same DESI lenses but different source samples, i.e., different source tomographic bins or lensing surveys. Specifically, if we have n lensing estimates μ_i with associated covariances Σ_i , the combined covariance is

$$\Sigma_{\text{tot}} = \left(\sum_{i=1}^n \Sigma_i^{-1} \right)^{-1} \quad (4)$$

and the combined estimate becomes

$$\mu_{\text{tot}} = \Sigma_{\text{tot}} \sum_{i=1}^n \Sigma_i^{-1} \mu_i. \quad (5)$$

We derive two sets of combined lensing measurements for each of the DESI samples. One set includes all lensing measurements from DES and KiDS and the other one the HSC measurements. Within the DESI footprint, DES and KiDS do not overlap spatially, allowing us to treat these measurements as independent. On the other hand, the HSC footprint in DESI overlaps with both DES and KiDS. Thus, the combined DES and KiDS lensing measurements have a non-zero covariance with the HSC measurements. In the following, we will refer to the combined DES and KiDS lensing measurements as DES/KiDS. The DES/KiDS footprints have a roughly $\sim 1,200 \text{ deg}^2$ overlap with DESI Y1 while HSC Y3 has a smaller $\sim 500 \text{ deg}^2$ overlap but higher source density.

Finally, the HSC Y3 lensing measurements are significantly affected by uncertainties in the photometric redshift calibration (Rau et al. 2023). In their $3 \times 2\text{pt}$ analysis, Li et al. (2023) used a self-calibration to show that applying an additional offset of $+0.115$ and $+0.192$ to the mean redshift of the third and forth tomographic bin, respectively, significantly improves the fit. A similar result was found by Heydenreich et al. (2025). Thus, by default, we assume these offsets to make our HSC Y3 lensing measurements. Later, we also discuss how our results would change if no offsets were applied to the fiducial HSC Y3 calibration in Rau et al. (2023).

3. METHODS

For the most part, our analysis method closely follows previous work by Lange et al. (2022, 2023) which we summarize here briefly.

3.1. Simulations

We start with a set of cosmological N -body simulations spanning a range of cosmologies, i.e., cosmological parameters. In previous work, the Aemulus Alpha simulations (DeRose et al. 2019) were used whereas we employ the AbacusSummit suite (Maksimova et al. 2021) in this work primarily due to its larger volume and higher resolution. From AbacusSummit, we select all cosmologies that vary Ω_m and σ_8 with respect to the base Planck Collaboration et al. (2020) CMB cosmology while keeping neutrino and dark energy properties as well as the shape of primordial power spectrum fixed. More explicitly, we use the cosmologies 0, 1, 4, 100, 101, 102, 103, 112, 113, 116, 117, 118, 125, 126, 130, 131, 133, and 134. Furthermore, we add the simulations 137, 140, and 144. While these do vary the spectral index n_s , they

Parameter	Description	Range
$\log M_{\min}$	Mass at which $\langle N_{\text{cen}} \rangle = 0.5$	[11, 15]
$\sigma_{\log M}$	Low-mass transition of $\langle N_{\text{cen}} \rangle$	[0.1, 1.0]
f_{Γ}	LRG incompleteness of $\langle N_{\text{cen}} \rangle$	[0.5, 1.0]
$\log M_0$	Mass below which $\langle N_{\text{sat}} \rangle = 0$	[11, 15]
$\log M_1$	Mass at which $\langle N_{\text{sat}} \rangle \approx 1$	[11, 15]
α	Power-law index of $\langle N_{\text{sat}} \rangle$	[0.5, 2.0]
A_{cen}	Central assembly bias	[-1.0, 1.0]
A_{sat}	Satellite assembly bias	[-1.0, 1.0]
$\log \eta$	Satellite spatial bias	[-0.5, 0.5]
α_s	Satellite velocity bias	[0.8, 1.2]

Table 1. Description and ranges of galaxy parameters varied in our analysis.

add important coverage in the Ω_m -direction. As shown in (Lange et al. 2023), the combination of projected clustering and lensing is not very sensitive to n_s and we neglect that n_s is varied in these simulations. The range of S_8 -range probed by these simulations is 0.73 to 0.93 and Ω_m goes from 0.255 to 0.388. Cosmological parameters related to the shape of the power spectrum are implicitly fixed in our cosmological analysis to the best-fitting values of the Planck Collaboration et al. (2020) CMB analysis¹.

For each cosmology, we select the base simulation with 6192³ particles and a volume of $(2h^{-1} \text{ Gpc})^3$, resulting in a particle resolution of $2.11 \times 10^9 (\Omega_m/0.314) h^{-1} M_{\odot}$. For each simulation, we use catalogs of all halos with at least 300 particles and a random 0.025% of all particles to sample the lensing field. These catalogs are extracted at redshifts 0.2, 0.3, 0.4, 0.5, and 0.8².

3.2. Galaxy Model

Halos in the AbacusSummit simulations are populated with galaxies via a Halo Occupation Distribution (HOD; Berlind & Weinberg 2002; Bullock et al. 2002; Zheng et al. 2007) model. The number of centrals, N_{cen} , per dark matter halo as a function of its halo mass M is given by

$$\langle N_{\text{cen}} | M \rangle = \frac{f_{\Gamma}}{2} \left(1 + \text{erf} \left[\frac{\log M - \log M_{\min}}{\sigma_{\log M}} \right] \right), \quad (6)$$

whereas the number of satellites, N_{sat} , obeys

$$\langle N_{\text{sat}} | M \rangle = \left(\frac{M - M_0}{M_1} \right)^{\alpha}. \quad (7)$$

¹ The different cosmological simulations also vary parameters such as H_0 and Ω_b . However, we interpret all changes in the goodness-of-fit as constraints on Ω_m and S_8 .

² Cosmology 103 does not have data for redshift 0.8. We do not use that cosmology for fits involving the high-redshift LRG2 sample.

In the above equations, f_{Γ} , $\log M_{\min}$, $\sigma_{\log M}$, M_0 , M_1 , and α are free parameters that we marginalize over in our analysis. The parameter f_{Γ} accounts for potential color incompleteness at high stellar masses for LRGs and is fixed to unity for the BGS samples.

The above parametrization describes a simple mass-only HOD and is supplemented with the decorated HOD framework (Hearin et al. 2016) to allow for galaxy assembly bias based on halo concentration. This gives two more free parameters, A_{cen} and A_{sat} , controlling the amount of assembly bias for centrals and satellites, respectively. Specifically, the number of centrals is modified based on the halo concentration c according to

$$\begin{aligned} \langle N_{\text{cen}} | M, c \rangle = \\ \langle N_{\text{cen}} | M \rangle \pm A_{\text{cen}} \min(\langle N_{\text{cen}} | M \rangle, 1 - \langle N_{\text{cen}} | M \rangle). \end{aligned} \quad (8)$$

In the above equation, the second term is added if the halo concentration is above the median concentration for halos of that mass and subtracted otherwise. Similarly, the satellite number becomes

$$\langle N_{\text{sat}} | M, c \rangle = \langle N_{\text{sat}} | M \rangle \pm A_{\text{sat}} \langle N_{\text{sat}} | M \rangle. \quad (9)$$

Both A_{cen} and A_{sat} are limited to the range $[-1, +1]$ to ensure the expected number of galaxies is always non-negative.

Finally, satellite positions and velocities are drawn from an analytic Navarro–Frenk–White (NFW; Navarro et al. 1997) profile with the second moment of the velocity distribution calculated from the time-independent Jeans equation. We allow satellites to have a biased spatial and velocity distribution with respect to the dark matter within each halo (see Lange et al. 2023, for details). The spatial bias is defined by $\eta = c_{\text{sat}}/c$, where c_{sat} is the concentration parameter of the satellite distribution within a halo. Similarly, α_s controls the velocity bias and represents an additional factor to multiply satellite velocities with.

We list all galaxy parameters together with a short description and the range of values we explore in our analysis in Table 1. The ranges explored are very broad and, in many cases, cover all values that meaningfully affect the predictions while being consistent with observations. Similarly, the limits for the assembly bias parameters are the maximum ranges allowed by the model (Hearin et al. 2016). While the ranges for $\log \eta$ and α_s could, in principle, be expanded, these parameters are virtually unconstrained by the data.

The above model allows us to place simulated galaxies into dark matter-only simulations. We then use the distant-observer approximation to measure galaxy clustering and lensing. For clustering, we take redshift-space

distortions into account. For lensing, we additionally make use of down-sampled particle catalogs to estimate the excess surface density $\Delta\Sigma$, using the algorithm outlined in Lange et al. (2019b). All mock measurements use the same binning as the real data and the clustering measurements include the Alcock-Paczynski effect (Alcock & Paczynski 1979), i.e., the assumed cosmology when converting redshifts and angles to physical coordinates. For lensing, the effect is expected to be small (More 2013) and is ignored.

We accelerate the prediction of galaxy clustering and lensing via TABCORR version 1.1.2. This software utilizes the tabulation method described in Zheng & Guo (2016); Lange et al. (2019a). In essence, we first calculate the clustering and lensing of central and satellite galaxies within halo mass and concentration bins. Afterward, the correlation functions are convolved with the HOD to make predictions for the galaxy correlation functions. Finally, we use cubic spline interpolation to make predictions for arbitrary phase-space parameters, i.e., $\log\eta$ and α_s , and redshifts. We checked that interpolation errors are small compared to observational uncertainties. Finally, we use the ‘efficient’ configuration in TABCORR to precompute the halo correlation functions.

Finally, we note two shortcomings in our galaxy model. Most importantly, we have implicitly neglected the impact of baryonic physics on the galaxy-galaxy lensing amplitude (see, e.g., Leauthaud et al. 2017; Lange et al. 2019b; Amodeo et al. 2021; Beltz-Mohrmann & Berlind 2021; Amon et al. 2023; Sunseri et al. 2025). Typically, neglecting baryonic processes will lead to an overprediction of the lensing amplitude on small scales. The scale cuts we impose are intended to mitigate this issue. We tested this by implementing the baryonic suppression of the lensing amplitude found by Lange et al. (2019b) for galaxies above a mass of $10^{11} M_\odot$ in the original Illustris simulation (Vogelsberger et al. 2014). Notably, the Illustris simulation already predicts a strong suppression due to baryonic feedback compared to other simulations (Amon & Eftathiou 2022). Nonetheless, we find that the baryonic suppression changes the final DES/KIDS constraints on S_8 and Ω_m by less than 0.2σ .

In addition to baryonic feedback, by drawing satellite positions from a smooth analytic density profile, we implicitly neglect the impact of subhalos (see, e.g., Zu & Mandelbaum 2015; Chaves-Montero et al. 2023) on the lensing amplitude. Unlike baryonic feedback, this simplification will lead to an underprediction of the lensing signal on small scales. However, as for baryonic feedback, the scale cut should substantially mitigate this is-

sue. Finally, we implement assembly bias based on halo concentration as the secondary halo property. However, recent works advocate for using other secondary halo properties such as over-density to model galaxy assembly bias (Xu et al. 2021; Hadzhiyska et al. 2021). Further tests are needed to determine whether using a different secondary halo property has a strong impact on our results.

3.3. Cosmological Inference

Starting with a set of observational data, $D_{\text{obs}} = \{n_{\text{gal}}, w_p, \Delta\Sigma\}$, our goal is to infer constraints on Ω_m and S_8 . The first step is to determine the best-fit, i.e., maximum-likelihood, galaxy model D_{mod} for each AbacusSummit simulation with respect to the observed data. The likelihood is defined as

$$\begin{aligned} \log \mathcal{L} &= -\frac{1}{2} \chi^2 \\ &= -\frac{1}{2} (D_{\text{obs}} - D_{\text{mod}})^T \Sigma^{-1} (D_{\text{obs}} - D_{\text{mod}}), \end{aligned} \quad (10)$$

where Σ is the covariance matrix of the observational data. We determine the maximum-likelihood galaxy model and posterior for each simulation using NAUTILUS (Lange 2023) with 3,000 live points and a stopping criterion of $f_{\text{live}} < 10^{-10}$. To determine cosmology constraints, in previous works (see, e.g., Lange et al. 2023), we ‘emulated’ the maximum likelihood $\log \mathcal{L}_{\text{max}}$ as a function of cosmology via skew-normal distributions. In this work, we opt for a different approach where we instead emulate the maximum-likelihood model predictions. We choose this method for its computational efficiency and to have a different method to test against. The observational S_8 constraints in this work do not change significantly with the skew-normal approach.

For each simulation representing different values for Ω_m and S_8 , we have the best-fit prediction D_m . First, we normalize these data vectors via $\tilde{D}_{\text{mod}} = D_{\text{mod}} / \sqrt{\text{diag}(\Sigma)}$ and reduce the dimensionality via a Principal Component Analysis (PCA). We only keep those N_{PCA} eigenvectors u_i that explain 99.9% of the variance across cosmology, typically the first 3 to 6 eigenvectors. Finally, we fit the cosmology dependence of each PCA component x_i via a simple linear model,

$$\hat{x}_i = a_i + b_i S_8 + c_i \Omega_m + d_i S_8^2. \quad (11)$$

We chose this specific linear model because it closely corresponds to a skew-normal likelihood, with a skew in the S_8 -dimension. This allows us to estimate the best-fit model D_{mod} , and thereby best-fit likelihood, for arbitrary values of Ω_m and S_8 . To account for uncertainties in this interpolation, we measure the leave-one-out scatter $\sigma_i^2 = \text{Var}(x_i - \hat{x}_i)$ between the linear model and the

actual values of the PCA components and add this to the covariance matrix,

$$\Sigma \rightarrow \Sigma + \sum_{i=1}^{N_{\text{PCA}}} \sigma_i^2 \left(u_i \sqrt{\text{diag}(\Sigma)} \right)^T \left(u_i \sqrt{\text{diag}(\Sigma)} \right). \quad (12)$$

Our results do not sensitively depend on the linear model or amount of variance considered in the PCA analysis since the emulation errors σ_{emu} are typically much smaller than the measurement uncertainties σ_{obs} . For example, for the DESI observational data, $\sigma_{\text{emu}} \lesssim 0.4 \sigma_{\text{obs}}$ for all samples and measurements. We tested a more flexible model in equation (11) by adding an $S_8 \times \Omega_m$ and an S_8^3 term but do not find significant differences for our observational constraints.

3.4. Verification

Before applying our analysis method to (masked) DESI data, we perform tests on simulated mock data to check for potential biases in our analysis method. The mock measurement are based on the DESI emulator mock challenge (Beltz-Mohrmann et al. in prep.). Mock galaxy catalogs are generated via the GalSampler method (Hearin et al. 2020) by transferring the galaxy-halo connection model from the diffksy model (Alarcon et al. 2023; Hearin et al. 2023) run on SMDPL simulation (Prada et al. 2012) to the UNIT simulations (Chuang et al. 2019).

As part of the DESI emulator mock challenge, LRG-like mocks were created at redshifts 0.5 and 0.8. Thus, to most closely mimic our analysis, we choose the 0.5 mock. However, that means that, unlike for the analysis of DESI data, we only use a single galaxy sample. From the available galaxy models, we choose the one where the GalSampler method use both halo mass and concentration. Furthermore, the intra-halo phase-space coordinates for galaxies use the host-centric model. We refer the reader to Beltz-Mohrmann et al. (in prep.) for more details about these simulations.

The mock catalogs are tuned to reproduce the properties of the BGS and LRG samples in the DESI Early Data Release (DESI Collaboration et al. 2024b). However, they do not include projections onto the sky or the actual DESI footprint. Instead, we use the distant observer approximation, averaging the results from the three simulation axes chosen as the line of sight. The covariance matrix used for inference is estimated using the jackknife method with 125 equal-volume parts each of the two UNIT simulation mocks. We note that uncertainties in these mock measurements, especially $\Delta\Sigma$, are much smaller than observational ones.

In Fig. 1, we show the best-fit galaxy model on the best-fit AbacusSummit simulation. We see that our

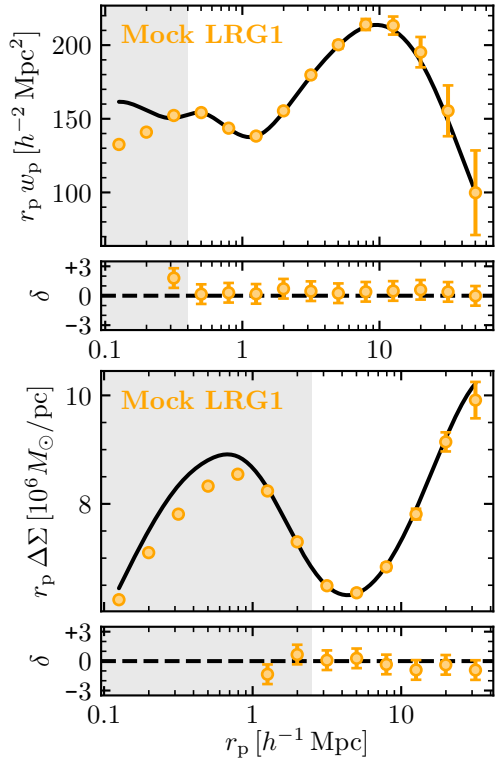


Figure 1. Best-fitting clustering and lensing predictions for the mock LRG1 measurements. The lower smaller panels indicate the difference between observations and model in units of the observational uncertainty. Gray regions indicate measurements not used in the fit.

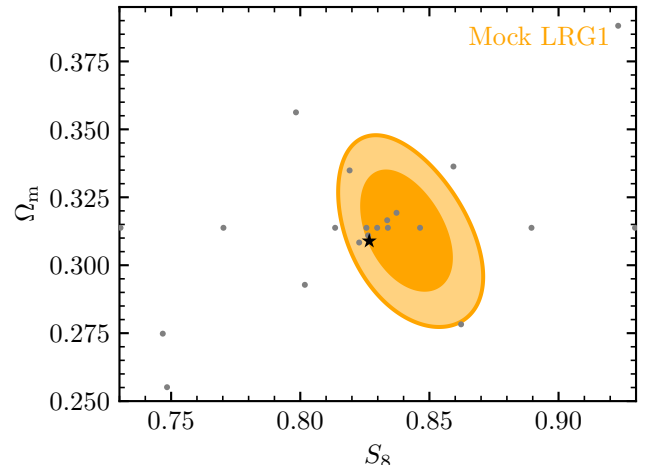


Figure 2. Mock constraints on S_8 and Ω_m . The different shaded regions indicate parameter spaces where $0 \leq \Delta\chi^2 < 2.28$ and $2.28 \leq \Delta\chi^2 < 5.99$ with respect to the best-fit cosmology, corresponding to the 68% and 95% confidence regions of a two-dimensional Gaussian distribution. The star indicates the values of S_8 and Ω_m in the UNIT simulations. Finally, small grey dots indicate the cosmological parameters of AbacusSummit simulations used in this analysis.

galaxy model can fit the mock data vector well with $\chi^2 = 11.8$ ($\chi^2_\nu = 11.8/(18 - 6.9 - 2)$, $p = 0.23$). In Fig. 2, we show the cosmological constraints in addition to the input cosmology of the UNIT simulations. We find that the UNIT cosmology is at $\Delta\chi^2 = 2.4$ from the best-fit cosmology. For reference, for a two-dimensional Gaussian, 31% of random draws will result in a higher $\Delta\chi^2$, indicating that our cosmological constraints are consistent with being unbiased. Nonetheless, we stress the need for additional mock tests in the future, especially for the BGS sample which may additionally be affected by the limited resolution of the AbacusSummit base simulations.

3.5. Masking

We aim to protect analysis choices in this work from confirmation bias and other subconscious effects that could bias the outcome of our analysis. To this end, we first perform “masked” analysis on the DESI data that allows us to implement quality controls, such as checking the goodness of fit, while being insensitive to the constraints on Ω_m and S_8 . We implement a data vector masking, similar to Muir et al. (2020) and Lange et al. (2023). We find that simply multiplying the lensing amplitude $\Delta\Sigma$ by an unknown factor A_{lens} , while keeping w_p unchanged, moves constraints mainly along the S_8 line while having only a small impact on the goodness of fit. Thus, to create the masked observational data, we draw A_{lens} from a uniform distribution in the range [0.85, 1.15] and multiply the lensing amplitudes for all DESI samples and lensing measurements by the same A_{lens} .

4. RESULTS

Here, we present the unmasked cosmology results. The results of this analysis were only unmasked after it was determined that the galaxy model can obtain an acceptable fit to the data and that the different DESI samples, BGS2, BGS3, LRG1, and LRG2, give consistent cosmological constraints.

4.1. Goodness of Fit

In Fig. 3, we show the best-fit model predictions for the different DESI samples studied in this work with lensing amplitudes from DES/KiDS. Fig. 4 shows a similar result but for lensing amplitudes from HSC. We find that we can obtain good fits to the data of all DESI lens samples with a single simulation, i.e., cosmology. The total goodness of fit is $\chi^2 = 50.7$ with 54 data points for DES/KiDS and $\chi^2 = 65.2$ with 72 data points for HSC. We have two degrees of freedom for the cosmology fit but the effective degrees of freedom of the galaxy

fit is significantly less than the number of galaxy model parameters since many are effectively unconstrained, as shown in Fig. 5. We estimate the effective degrees of freedom numerically. We start with the best-fit galaxy model θ_0 for each sample at AbacusSummit cosmology 0. We then repeatedly draw mock observations from a multivariate normal distribution with the predictions from θ_0 as the mean and the observational uncertainties as the covariance. Finally, we minimize the χ^2 over the galaxy parameters and calculate the difference between the minimum χ^2 and $\chi^2(\theta_0)$. Based on the reduction in the χ^2 , we estimate the effective degrees of freedom in the galaxy parameters over all DESI samples to be around 14.0 for the DES/KiDS fits and 20.3 for the HSC fits. This gives $\chi^2_\nu = 51.6/38.0$ ($p = 0.08$) for DES/KiDS and $\chi^2_\nu = 65.2/49.7$ ($p = 0.07$) for HSC. Overall, this indicates an acceptable fit of our Λ CDM and HOD-based model to the observational data.

4.2. Cosmology

The main result of our analysis, observational constraints on S_8 and Ω_m , are shown in Fig. 6. We show the individual constraints from the different samples as well as their combination. The best-fit χ^2 when fitting all samples with a single combination of S_8 and Ω_m increases by $\Delta\chi^2 = 5.0$ for DES/KiDS and 4.2 for HSC compared to optimizing those two parameters for each individual sample. This increase in χ^2 is consistent with reducing the degrees of freedom by 4 for DES/KiDS ($\Delta\chi^2_\nu = 5.0/4$, $p = 0.29$) and 6 for HSC ($\Delta\chi^2_\nu = 5.8/6$, $p = 0.65$), indicating that the different DESI samples produce consistent results on S_8 and Ω_m . Our final marginalized (Frequentist) constraints are $S_8 = 0.794 \pm 0.023$ and $\Omega_m = 0.295 \pm 0.012$ for DES/KiDS and $S_8 = 0.793 \pm 0.017$ and $\Omega_m = 0.303 \pm 0.010$ for HSC.

For HSC, the constraints listed above assume the best-fit photometric redshift offsets found by Li et al. (2023). If we assume no offsets, we find $S_8 = 0.842 \pm 0.018$ and $\Omega_m = 0.307 \pm 0.010$, instead. However, the total χ^2 increases by 6.6, indicating that this scenario is disfavored by the data. Given the shift of $\Delta S_8 = 0.048$ with $\Delta\chi^2 = 6.6$, we estimate that a full marginalization over photometric redshift calibration uncertainties would roughly add $\sim \Delta S_8 / \sqrt{\Delta\chi^2} = 0.019$ to the overall uncertainty in S_8 . In other words, the results for HSC are likely limited by systematic uncertainties in the photometric redshift calibration.

Finally, we compare our results derived here against the Planck Collaboration et al. (2020) CMB results in Fig. 7. Overall, our results are consistent with the

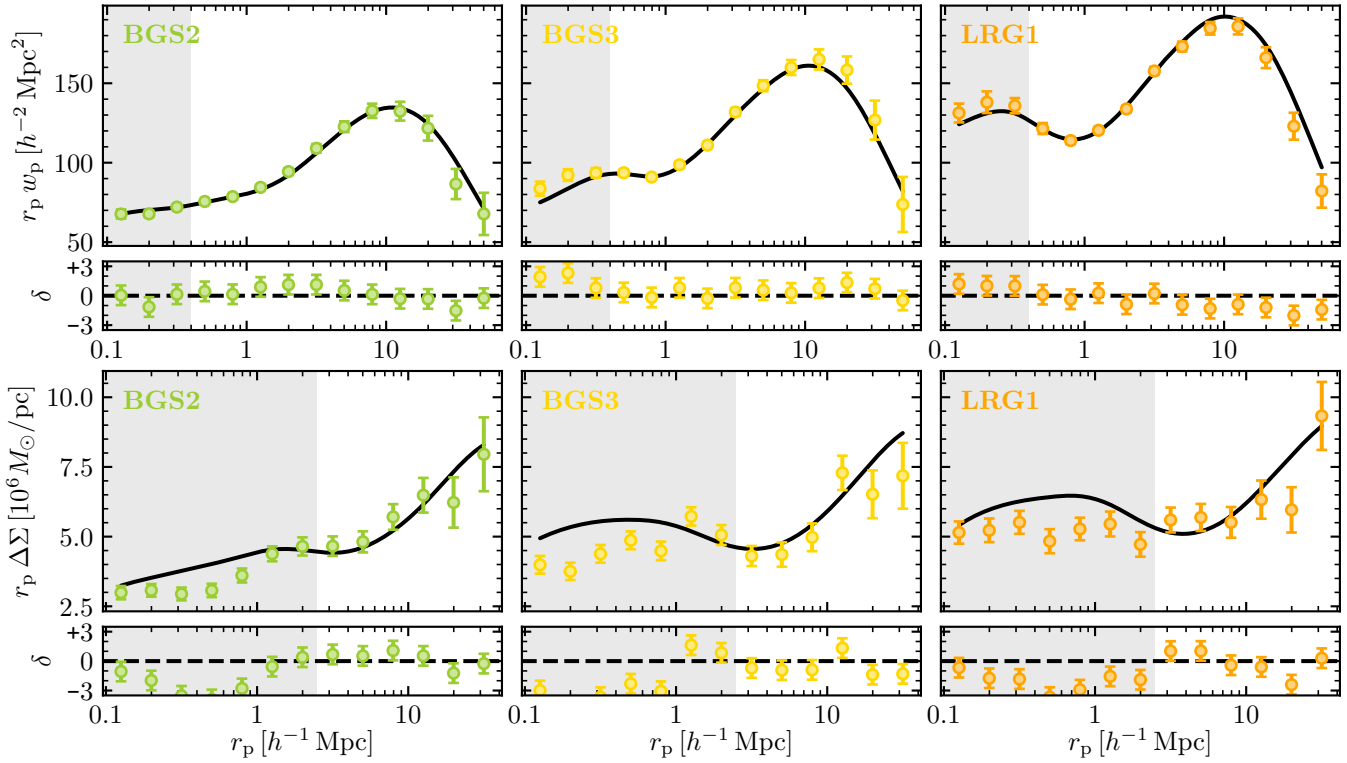


Figure 3. Similar to Fig 1 but for the DESI measurements with DES and KiDS lensing. The best-fit simulation, `AbacusSummit_base_c103.ph000`, is the one that minimizes the total χ^2 of all three samples whereas the galaxy model is optimized individually for each sample.

[Planck Collaboration et al. \(2020\)](#) constraints albeit preferring a lower value for S_8 .

5. CONCLUSION

In this work, we present new constraints of cosmic structure growth from the analysis of non-linear clustering and galaxy-galaxy lensing with DESI DR1. We implement a complex, simulation-based modeling framework that accounts for important details in the galaxy-halo connection such as galaxy assembly bias. Overall, our results align well with previous literature results. In particular, comparing with Porredon et al. (in prep.), we find that the analysis of non-linear scales substantially improves the cosmological constraining power of the data (see, e.g., [Reid et al. 2014](#); [Wibking et al. 2019](#); [Lange et al. 2022](#)). However, it is worth re-emphasizing that we fix cosmological parameters other than S_8 and Ω_m to the best-fit CMB values instead of marginalizing over them.

Our analysis places stringent constraints on cosmic structure growth, particularly the S_8 parameter. While our maximum-likelihood value for S_8 falls below that of the [Planck Collaboration et al. \(2020\)](#) CMB analysis, similar to many other low-redshift studies ([Abdalla et al. 2022](#)), our results are also not in significant tension with CMB results. This finding is similar to other re-

cent studies of non-linear clustering and lensing lensing ([Wibking et al. 2020](#); [Dvornik et al. 2023](#); [Amon et al. 2023](#); [Lange et al. 2023](#)). Our results also align with earlier studies reporting the so-called lensing-is-low problem ([Leauthaud et al. 2017](#); [Lange et al. 2019b](#)). This problem arises when comparing the lensing amplitude on very small scales, down to $0.1 h^{-1} \text{Mpc}$, to predictions of simple mass-only HOD models and without the expected impact of baryons. In this work, we take into account assembly bias and do not model the scales expected to be most strongly affected by baryonic physics. Indeed, looking at Figs. 3 and 4, we see that our best-fit models consistently overpredict lensing amplitude below $1 h^{-1} \text{Mpc}$.

The present work serves as a precursor for future studies with DESI data that promise further increases in statistical constraining power. To fully realize this potential, further steps need to be taken to reduce systematic and modeling uncertainties. In the current analysis, we exclude the lensing signal on scales below $2.5 h^{-1} \text{Mpc}$ from the analysis due to the potential impact of baryonic physics. If we were to constrain baryonic feedback, we could potentially make use of the high-precision lensing measurements on these very small scales. Similarly, despite advances in recent years, further mock tests

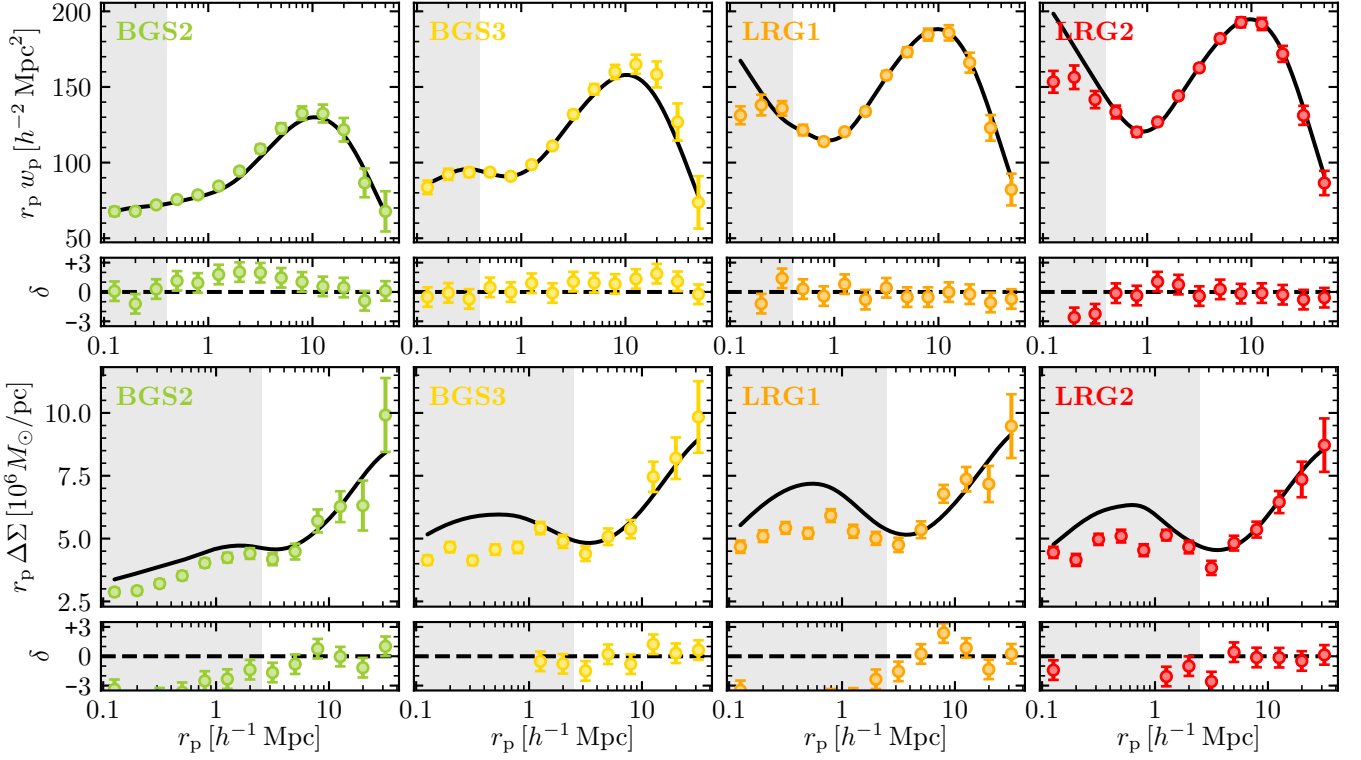


Figure 4. Similar to Fig 3 but for the DESI measurements with HSC lensing amplitudes. The best-fitting simulation is AbacusSummit_base_c118_ph000.

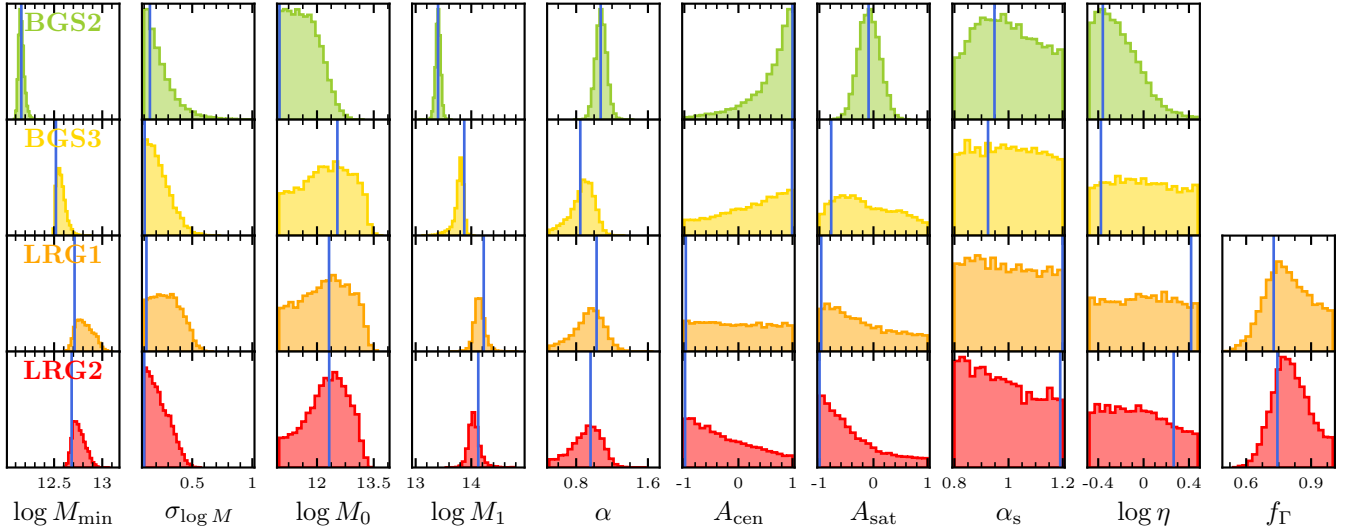


Figure 5. One-dimensional Bayesian posteriors on the galaxy model parameters for the four DESI samples with HSC lensing amplitudes under the best-fit cosmology. We also show the best-fit parameters as blue vertical lines. The different parameters are described in 1.

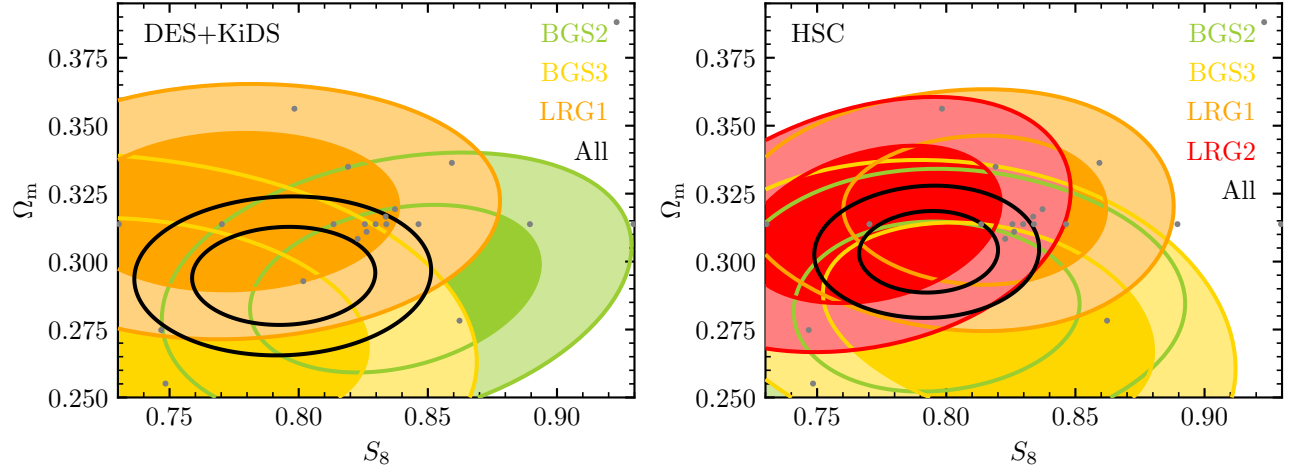


Figure 6. Observational constraints on S_8 and Ω_m for DESI clustering measurements combined with DES Y3 and KiDS-1000 lensing measurements (left) and HSC Y3 lensing amplitudes (right). The different shaded regions demarcate that $\Delta\chi^2 = 2.28$ and $\Delta\chi^2 = 5.99$ boundaries. The black contour indicates the combined results by adding the χ^2 contributions from the individual samples.

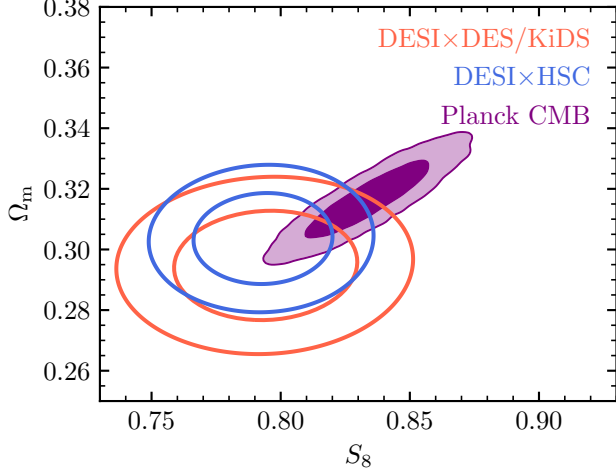


Figure 7. Comparison of the constraints derived in this work against the (Planck Collaboration et al. 2020) CMB results. The purple contours show the 68% and 95% containment ranges of the TT,TE,EE+lowE CMB analysis and have been smoothed for clarity.

should be conducted to investigate the robustness of cosmological constraints from non-linear scales (Doytcheva et al. 2024; ThBeyond-2pt Collaboration et al. 2025; Zhai et al. 2025). Finally, specifically for gravitational lensing with HSC, reducing uncertainties in the photometric redshift calibration is critical.

In the future, joint studies of clustering, lensing, and the Sunyaev-Zel'dovich effect could significantly reduce the uncertainty on baryonic physics and allow us to model smaller scales (Amodeo et al. 2021; Sunseri et al. 2025). In particular, the overlap of DESI with the footprint of the Atacama Cosmology Telescope (ACT) enables high-precision measurements of the kinetic Sunyaev-Zel'dovich effect (Hadzhiyska et al. 2025). Similarly, DESI is an excellent source for high-quality spectroscopic redshifts that will allow us to reduce uncertainties in the HSC photometric redshift calibration. This can be done both via clustering redshifts using DESI large-scale structure catalogs (Choppin de Janvry et al. 2025; Ruggeri et al. in prep.) and direct calibration using DESI redshifts in deep drilling fields (Ratajczak et al. 2025; Lange et al. 2025).

DATA AVAILABILITY

All data points shown in the published graphs will be available at <https://zenodo.org/records/17831718> upon publication. We have released all TABCORR data products used in this work to the community at <https://zenodo.org/records/15588541> as part of the TABCORR library.

ACKNOWLEDGMENTS

This work made use of the following software packages: ASTROPY (Astropy Collaboration et al. 2013, 2018, 2022), CORRFUNC (Sinha & Garrison 2020), HALO_TOOLS (Hearin et al. 2017), MATPLOTLIB (Hunter 2007), NUMPY (Van Der Walt et al. 2011), SciPY (Virtanen et al. 2020), TABCORR (Lange et al. 2019a), and SPYDER.

This material is based upon work supported by the U.S. Department of Energy (DOE), Office of Science, Office of High-Energy Physics, under Contract No. DE-AC02-05CH11231, and by the National Energy Research Scientific Computing Center, a DOE Office of Science User Facility under the same contract. Additional support for DESI was provided by the U.S. National Science Foundation (NSF), Division of Astronomical Sciences under Contract No. AST-0950945 to the NSF's National Optical-Infrared Astronomy Research Laboratory; the Science and Technology Facilities Council of the United Kingdom; the Gordon and Betty Moore Foundation; the Heising-Simons Foundation; the French Alternative Energies and Atomic Energy Commission (CEA); the National Council of Humanities, Science and Technology of Mexico (CONAH-CYT); the Ministry of Science, Innovation and Universities of Spain (MICIU/AEI/10.13039/501100011033), and by the DESI Member Institutions: <https://www.desi.lbl.gov/collaborating-institutions>. Any opinions, findings, and conclusions or recommendations expressed in this material are those of the author(s) and do not necessarily reflect the views of the U. S. National Science Foundation, the U. S. Department of Energy, or any of the listed funding agencies.

The authors are honored to be permitted to conduct scientific research on I'oligam Du'ag (Kitt Peak), a mountain with particular significance to the Tohono O'odham Nation.

REFERENCES

Abbott, T. M. C., Aguena, M., Alarcon, A., et al. 2022, PhRvD, 105, 023520, doi: [10.1103/PhysRevD.105.023520](https://doi.org/10.1103/PhysRevD.105.023520)

Abdalla, E., Abellán, G. F., Aboubrahim, A., et al. 2022, Journal of High Energy Astrophysics, 34, 49, doi: [10.1016/j.jheap.2022.04.002](https://doi.org/10.1016/j.jheap.2022.04.002)

Abdul Karim, M., Aguilar, J., Ahlen, S., et al. 2025, *PhRvD*, 112, 083515, doi: [10.1103/tr6y-kpc6](https://doi.org/10.1103/tr6y-kpc6)

Adame, A. G., Aguilar, J., Ahlen, S., et al. 2025a, *JCAP*, 2025, 028, doi: [10.1088/1475-7516/2025/07/028](https://doi.org/10.1088/1475-7516/2025/07/028)

—. 2025b, *JCAP*, 2025, 017, doi: [10.1088/1475-7516/2025/07/017](https://doi.org/10.1088/1475-7516/2025/07/017)

Ahumada, R., Allende Prieto, C., Almeida, A., et al. 2020, *ApJS*, 249, 3, doi: [10.3847/1538-4365/ab929e](https://doi.org/10.3847/1538-4365/ab929e)

Aihara, H., Arimoto, N., Armstrong, R., et al. 2018, *PASJ*, 70, S4, doi: [10.1093/pasj/psx066](https://doi.org/10.1093/pasj/psx066)

Alarcon, A., Hearin, A. P., Becker, M. R., & Chaves-Montero, J. 2023, *MNRAS*, 518, 562, doi: [10.1093/mnras/stac3118](https://doi.org/10.1093/mnras/stac3118)

Alcock, C., & Paczynski, B. 1979, *Nature*, 281, 358, doi: [10.1038/281358a0](https://doi.org/10.1038/281358a0)

Amodeo, S., Battaglia, N., Schaan, E., et al. 2021, *PhRvD*, 103, 063514, doi: [10.1103/PhysRevD.103.063514](https://doi.org/10.1103/PhysRevD.103.063514)

Amon, A., & Efstathiou, G. 2022, *MNRAS*, 516, 5355, doi: [10.1093/mnras/stac2429](https://doi.org/10.1093/mnras/stac2429)

Amon, A., Robertson, N. C., Miyatake, H., et al. 2023, *MNRAS*, 518, 477, doi: [10.1093/mnras/stac2938](https://doi.org/10.1093/mnras/stac2938)

Asgari, M., Lin, C.-A., Joachimi, B., et al. 2021, *A&A*, 645, A104, doi: [10.1051/0004-6361/202039070](https://doi.org/10.1051/0004-6361/202039070)

Astropy Collaboration, Robitaille, T. P., Tollerud, E. J., et al. 2013, *A&A*, 558, A33, doi: [10.1051/0004-6361/201322068](https://doi.org/10.1051/0004-6361/201322068)

Astropy Collaboration, Price-Whelan, A. M., Sipőcz, B. M., et al. 2018, *AJ*, 156, 123, doi: [10.3847/1538-3881/aabc4f](https://doi.org/10.3847/1538-3881/aabc4f)

Astropy Collaboration, Price-Whelan, A. M., Lim, P. L., et al. 2022, *ApJ*, 935, 167, doi: [10.3847/1538-4357/ac7c74](https://doi.org/10.3847/1538-4357/ac7c74)

Beltz-Mohrmann, G. D., & Berlind, A. A. 2021, *ApJ*, 921, 112, doi: [10.3847/1538-4357/ac1e27](https://doi.org/10.3847/1538-4357/ac1e27)

Berlind, A. A., & Weinberg, D. H. 2002, *ApJ*, 575, 587, doi: [10.1086/341469](https://doi.org/10.1086/341469)

Bianchi, D., Burden, A., Percival, W. J., et al. 2018, *MNRAS*, 481, 2338, doi: [10.1093/mnras/sty2377](https://doi.org/10.1093/mnras/sty2377)

Bianchi, D., Hanif, M. M. S., Carnero Rosell, A., et al. 2025, *JCAP*, 2025, 074, doi: [10.1088/1475-7516/2025/04/074](https://doi.org/10.1088/1475-7516/2025/04/074)

Bullock, J. S., Wechsler, R. H., & Somerville, R. S. 2002, *MNRAS*, 329, 246, doi: [10.1046/j.1365-8711.2002.04959.x](https://doi.org/10.1046/j.1365-8711.2002.04959.x)

Cacciato, M., van den Bosch, F. C., More, S., Mo, H., & Yang, X. 2013, *MNRAS*, 430, 767, doi: [10.1093/mnras/sts525](https://doi.org/10.1093/mnras/sts525)

Chaves-Montero, J., Angulo, R. E., & Contreras, S. 2023, *MNRAS*, 521, 937, doi: [10.1093/mnras/stad243](https://doi.org/10.1093/mnras/stad243)

Choppin de Janvry, J., Gontcho, S. G. A., Seljak, U., et al. 2025, arXiv e-prints, arXiv:2511.18133, doi: [10.48550/arXiv.2511.18133](https://doi.org/10.48550/arXiv.2511.18133)

Chuang, C.-H., Yepes, G., Kitaura, F.-S., et al. 2019, *MNRAS*, 487, 48, doi: [10.1093/mnras/stz1233](https://doi.org/10.1093/mnras/stz1233)

DeRose, J., Wechsler, R. H., Tinker, J. L., et al. 2019, *ApJ*, 875, 69, doi: [10.3847/1538-4357/ab1085](https://doi.org/10.3847/1538-4357/ab1085)

DESI Collaboration, Aghamousa, A., Aguilar, J., et al. 2016a, arXiv e-prints, arXiv:1611.00036, doi: [10.48550/arXiv.1611.00036](https://doi.org/10.48550/arXiv.1611.00036)

—. 2016b, arXiv e-prints, arXiv:1611.00037, doi: [10.48550/arXiv.1611.00037](https://doi.org/10.48550/arXiv.1611.00037)

DESI Collaboration, Abareshi, B., Aguilar, J., et al. 2022, *AJ*, 164, 207, doi: [10.3847/1538-3881/ac882b](https://doi.org/10.3847/1538-3881/ac882b)

DESI Collaboration, Adame, A. G., Aguilar, J., et al. 2024a, *AJ*, 167, 62, doi: [10.3847/1538-3881/ad0b08](https://doi.org/10.3847/1538-3881/ad0b08)

—. 2024b, *AJ*, 168, 58, doi: [10.3847/1538-3881/ad3217](https://doi.org/10.3847/1538-3881/ad3217)

DESI Collaboration, Abdul-Karim, M., Adame, A. G., et al. 2025, arXiv e-prints, arXiv:2503.14745, doi: [10.48550/arXiv.2503.14745](https://doi.org/10.48550/arXiv.2503.14745)

Doytcheva, A., Gerou, F. V., & Lange, J. U. 2024, *ApJ*, 977, 184, doi: [10.3847/1538-4357/ad919d](https://doi.org/10.3847/1538-4357/ad919d)

Dvornik, A., Heymans, C., Asgari, M., et al. 2023, *A&A*, 675, A189, doi: [10.1051/0004-6361/202245158](https://doi.org/10.1051/0004-6361/202245158)

Flaughher, B., Diehl, H. T., Honscheid, K., et al. 2015, *AJ*, 150, 150, doi: [10.1088/0004-6256/150/5/150](https://doi.org/10.1088/0004-6256/150/5/150)

Gatti, M., Sheldon, E., Amon, A., et al. 2021, *MNRAS*, 504, 4312, doi: [10.1093/mnras/stab918](https://doi.org/10.1093/mnras/stab918)

Giblin, B., Heymans, C., Asgari, M., et al. 2021, *A&A*, 645, A105, doi: [10.1051/0004-6361/202038850](https://doi.org/10.1051/0004-6361/202038850)

Guy, J., Bailey, S., Kremin, A., et al. 2023, *AJ*, 165, 144, doi: [10.3847/1538-3881/acb212](https://doi.org/10.3847/1538-3881/acb212)

Hadzhiyska, B., Liu, S., Somerville, R. S., et al. 2021, *MNRAS*, 508, 698, doi: [10.1093/mnras/stab2564](https://doi.org/10.1093/mnras/stab2564)

Hadzhiyska, B., Ferraro, S., Ried Guachalla, B., et al. 2025, *PhRvD*, 112, 083509, doi: [10.1103/kclp-x5j1](https://doi.org/10.1103/kclp-x5j1)

Hahn, C., & Villaescusa-Navarro, F. 2021, *JCAP*, 2021, 029, doi: [10.1088/1475-7516/2021/04/029](https://doi.org/10.1088/1475-7516/2021/04/029)

Hahn, C., Lemos, P., Parker, L., et al. 2023a, arXiv e-prints, arXiv:2310.15246, doi: [10.48550/arXiv.2310.15246](https://doi.org/10.48550/arXiv.2310.15246)

Hahn, C., Wilson, M. J., Ruiz-Macias, O., et al. 2023b, *AJ*, 165, 253, doi: [10.3847/1538-3881/acff8](https://doi.org/10.3847/1538-3881/acff8)

Hartlap, J., Simon, P., & Schneider, P. 2007, *A&A*, 464, 399, doi: [10.1051/0004-6361:20066170](https://doi.org/10.1051/0004-6361:20066170)

Hearin, A., Korytov, D., Kovacs, E., et al. 2020, *MNRAS*, 495, 5040, doi: [10.1093/mnras/staa1495](https://doi.org/10.1093/mnras/staa1495)

Hearin, A. P., Chaves-Montero, J., Alarcon, A., Becker, M. R., & Benson, A. 2023, *MNRAS*, 521, 1741, doi: [10.1093/mnras/stad456](https://doi.org/10.1093/mnras/stad456)

Hearin, A. P., Zentner, A. R., van den Bosch, F. C., Campbell, D., & Tollerud, E. 2016, *MNRAS*, 460, 2552, doi: [10.1093/mnras/stw840](https://doi.org/10.1093/mnras/stw840)

Hearin, A. P., Campbell, D., Tollerud, E., et al. 2017, *AJ*, 154, 190, doi: [10.3847/1538-3881/aa859f](https://doi.org/10.3847/1538-3881/aa859f)

Heydenreich, S., Leauthaud, A., Blake, C., et al. 2025, arXiv e-prints, arXiv:2506.21677, doi: [10.48550/arXiv.2506.21677](https://doi.org/10.48550/arXiv.2506.21677)

Hunter, J. D. 2007, Computing in Science and Engineering, 9, 90, doi: [10.1109/MCSE.2007.55](https://doi.org/10.1109/MCSE.2007.55)

Ishak, M., Pan, J., Calderon, R., et al. 2025, JCAP, 2025, 053, doi: [10.1088/1475-7516/2025/09/053](https://doi.org/10.1088/1475-7516/2025/09/053)

Ivanov, M. M., Obuljen, A., Cuesta-Lazaro, C., & Toomey, M. W. 2025, PhRvD, 111, 063548, doi: [10.1103/PhysRevD.111.063548](https://doi.org/10.1103/PhysRevD.111.063548)

Kuijken, K., Heymans, C., Hildebrandt, H., et al. 2015, MNRAS, 454, 3500, doi: [10.1093/mnras/stv2140](https://doi.org/10.1093/mnras/stv2140)

Lange, J. U. 2023, MNRAS, 525, 3181, doi: [10.1093/mnras/stad2441](https://doi.org/10.1093/mnras/stad2441)

Lange, J. U., Hearin, A. P., Leauthaud, A., et al. 2022, MNRAS, 509, 1779, doi: [10.1093/mnras/stab3111](https://doi.org/10.1093/mnras/stab3111)

—. 2023, MNRAS, 520, 5373, doi: [10.1093/mnras/stad473](https://doi.org/10.1093/mnras/stad473)

Lange, J. U., van den Bosch, F. C., Zentner, A. R., et al. 2019a, MNRAS, 490, 1870, doi: [10.1093/mnras/stz2664](https://doi.org/10.1093/mnras/stz2664)

Lange, J. U., Yang, X., Guo, H., Luo, W., & van den Bosch, F. C. 2019b, MNRAS, 488, 5771, doi: [10.1093/mnras/stz2124](https://doi.org/10.1093/mnras/stz2124)

Lange, J. U., Blake, C., Saulder, C., et al. 2024, The Open Journal of Astrophysics, 7, 57, doi: [10.33232/001c.121260](https://doi.org/10.33232/001c.121260)

Lange, J. U., Blanco, D., Leauthaud, A., et al. 2025, arXiv e-prints, arXiv:2510.25419, doi: [10.48550/arXiv.2510.25419](https://doi.org/10.48550/arXiv.2510.25419)

Leauthaud, A., Saito, S., Hilbert, S., et al. 2017, MNRAS, 467, 3024, doi: [10.1093/mnras/stx258](https://doi.org/10.1093/mnras/stx258)

Levi, M., Bebek, C., Beers, T., et al. 2013, arXiv e-prints, arXiv:1308.0847, doi: [10.48550/arXiv.1308.0847](https://doi.org/10.48550/arXiv.1308.0847)

Li, X., Miyatake, H., Luo, W., et al. 2022, PASJ, 74, 421, doi: [10.1093/pasj/psac006](https://doi.org/10.1093/pasj/psac006)

Li, X., Zhang, T., Sugiyama, S., et al. 2023, PhRvD, 108, 123518, doi: [10.1103/PhysRevD.108.123518](https://doi.org/10.1103/PhysRevD.108.123518)

Liu, W., Paillas, E., Cuesta-Lazaro, C., Valogiannis, G., & Fang, W. 2025, JCAP, 2025, 064, doi: [10.1088/1475-7516/2025/05/064](https://doi.org/10.1088/1475-7516/2025/05/064)

Maksimova, N. A., Garrison, L. H., Eisenstein, D. J., et al. 2021, MNRAS, 508, 4017, doi: [10.1093/mnras/stab2484](https://doi.org/10.1093/mnras/stab2484)

Miller, T. N., Doel, P., Gutierrez, G., et al. 2024, AJ, 168, 95, doi: [10.3847/1538-3881/ad45fe](https://doi.org/10.3847/1538-3881/ad45fe)

Miyatake, H., Sugiyama, S., Takada, M., et al. 2023, PhRvD, 108, 123517, doi: [10.1103/PhysRevD.108.123517](https://doi.org/10.1103/PhysRevD.108.123517)

More, S. 2013, ApJL, 777, L26, doi: [10.1088/2041-8205/777/2/L26](https://doi.org/10.1088/2041-8205/777/2/L26)

More, S., Sugiyama, S., Miyatake, H., et al. 2023, PhRvD, 108, 123520, doi: [10.1103/PhysRevD.108.123520](https://doi.org/10.1103/PhysRevD.108.123520)

Moustakas, J., Buhler, J., Scholte, D., Dey, B., & Khederlarian, A. 2023, FastSpecFit: Fast spectral synthesis and emission-line fitting of DESI spectra, Astrophysics Source Code Library, record ascl:2308.005. <http://ascl.net/2308.005>

Muir, J., Bernstein, G. M., Huterer, D., et al. 2020, MNRAS, 494, 4454, doi: [10.1093/mnras/staa965](https://doi.org/10.1093/mnras/staa965)

Navarro, J. F., Frenk, C. S., & White, S. D. M. 1997, ApJ, 490, 493, doi: [10.1086/304888](https://doi.org/10.1086/304888)

Nguyen, N.-M., Schmidt, F., Tucci, B., Reinecke, M., & Kostić, A. 2024, PhRvL, 133, 221006, doi: [10.1103/PhysRevLett.133.221006](https://doi.org/10.1103/PhysRevLett.133.221006)

Planck Collaboration, Ade, P. A. R., Aghanim, N., et al. 2016, A&A, 594, A24, doi: [10.1051/0004-6361/201525833](https://doi.org/10.1051/0004-6361/201525833)

Planck Collaboration, Aghanim, N., Akrami, Y., et al. 2020, A&A, 641, A6, doi: [10.1051/0004-6361/201833910](https://doi.org/10.1051/0004-6361/201833910)

Poppett, C., Tyas, L., Aguilar, J., et al. 2024, AJ, 168, 245, doi: [10.3847/1538-3881/ad76a4](https://doi.org/10.3847/1538-3881/ad76a4)

Prada, F., Klypin, A. A., Cuesta, A. J., Betancort-Rijo, J. E., & Primack, J. 2012, MNRAS, 423, 3018, doi: [10.1111/j.1365-2966.2012.21007.x](https://doi.org/10.1111/j.1365-2966.2012.21007.x)

Ratajczak, J., Dawson, K. S., Weaverdyck, N., et al. 2025, arXiv e-prints, arXiv:2508.09286, doi: [10.48550/arXiv.2508.09286](https://doi.org/10.48550/arXiv.2508.09286)

Rau, M. M., Dalal, R., Zhang, T., et al. 2023, MNRAS, 524, 5109, doi: [10.1093/mnras/stad1962](https://doi.org/10.1093/mnras/stad1962)

Reid, B., Ho, S., Padmanabhan, N., et al. 2016, MNRAS, 455, 1553, doi: [10.1093/mnras/stv2382](https://doi.org/10.1093/mnras/stv2382)

Reid, B. A., Seo, H.-J., Leauthaud, A., Tinker, J. L., & White, M. 2014, MNRAS, 444, 476, doi: [10.1093/mnras/stu1391](https://doi.org/10.1093/mnras/stu1391)

Schlafly, E. F., Kirkby, D., Schlegel, D. J., et al. 2023, AJ, 166, 259, doi: [10.3847/1538-3881/ad0832](https://doi.org/10.3847/1538-3881/ad0832)

Silber, J. H., Fagrelius, P., Fanning, K., et al. 2023, AJ, 165, 9, doi: [10.3847/1538-3881/ac9ab1](https://doi.org/10.3847/1538-3881/ac9ab1)

Sinha, M., & Garrison, L. H. 2020, MNRAS, 491, 3022, doi: [10.1093/mnras/stz3157](https://doi.org/10.1093/mnras/stz3157)

Springel, V., Pakmor, R., Pillepich, A., et al. 2018, MNRAS, 475, 676, doi: [10.1093/mnras/stx3304](https://doi.org/10.1093/mnras/stx3304)

Sugiyama, S., Miyatake, H., More, S., et al. 2023, PhRvD, 108, 123521, doi: [10.1103/PhysRevD.108.123521](https://doi.org/10.1103/PhysRevD.108.123521)

Sunseri, J., Amon, A., Dunkley, J., et al. 2025, arXiv e-prints, arXiv:2505.20413, doi: [10.48550/arXiv.2505.20413](https://doi.org/10.48550/arXiv.2505.20413)

ThBeyond-2pt Collaboration, Krause, E., Kobayashi, Y., et al. 2025, ApJ, 990, 99, doi: [10.3847/1538-4357/ad781d](https://doi.org/10.3847/1538-4357/ad781d)

Unruh, S., Schneider, P., Hilbert, S., et al. 2020, A&A, 638, A96, doi: [10.1051/0004-6361/201936915](https://doi.org/10.1051/0004-6361/201936915)

Valogiannis, G., Yuan, S., & Dvorkin, C. 2024, PhRvD, 109, 103503, doi: [10.1103/PhysRevD.109.103503](https://doi.org/10.1103/PhysRevD.109.103503)

van Daalen, M. P., McCarthy, I. G., & Schaye, J. 2020, MNRAS, 491, 2424, doi: [10.1093/mnras/stz3199](https://doi.org/10.1093/mnras/stz3199)

van Daalen, M. P., Schaye, J., Booth, C. M., & Dalla Vecchia, C. 2011, MNRAS, 415, 3649, doi: [10.1111/j.1365-2966.2011.18981.x](https://doi.org/10.1111/j.1365-2966.2011.18981.x)

Van Der Walt, S., Colbert, S. C., & Varoquaux, G. 2011, Computing in Science and Engineering, 13, 22, doi: [10.1109/MCSE.2011.37](https://doi.org/10.1109/MCSE.2011.37)

Virtanen, P., Gommers, R., Oliphant, T. E., et al. 2020, Nature Medicine, 17, 261, doi: [10.1038/s41592-019-0686-2](https://doi.org/10.1038/s41592-019-0686-2)

Vogelsberger, M., Genel, S., Springel, V., et al. 2014, MNRAS, 444, 1518, doi: [10.1093/mnras/stu1536](https://doi.org/10.1093/mnras/stu1536)

Wechsler, R. H., & Tinker, J. L. 2018, ARA&A, 56, 435, doi: [10.1146/annurev-astro-081817-051756](https://doi.org/10.1146/annurev-astro-081817-051756)

Wibking, B. D., Weinberg, D. H., Salcedo, A. N., et al. 2020, MNRAS, 492, 2872, doi: [10.1093/mnras/stz3423](https://doi.org/10.1093/mnras/stz3423)

Wibking, B. D., Salcedo, A. N., Weinberg, D. H., et al. 2019, MNRAS, 484, 989, doi: [10.1093/mnras/sty2258](https://doi.org/10.1093/mnras/sty2258)

Wright, A. H., Stölzner, B., Asgari, M., et al. 2025, A&A, 703, A158, doi: [10.1051/0004-6361/202554908](https://doi.org/10.1051/0004-6361/202554908)

Xu, X., Zehavi, I., & Contreras, S. 2021, MNRAS, 502, 3242, doi: [10.1093/mnras/stab100](https://doi.org/10.1093/mnras/stab100)

Yuan, S., Garrison, L. H., Eisenstein, D. J., & Wechsler, R. H. 2022, MNRAS, 515, 871, doi: [10.1093/mnras/stac1830](https://doi.org/10.1093/mnras/stac1830)

Yuan, S., Blake, C., Krolewski, A., et al. 2024, MNRAS, 533, 589, doi: [10.1093/mnras/stae1792](https://doi.org/10.1093/mnras/stae1792)

Zhai, Z., Benson, A., & Wang, Y. 2025, MNRAS, 544, 932, doi: [10.1093/mnras/staf1774](https://doi.org/10.1093/mnras/staf1774)

Zhai, Z., Tinker, J. L., Banerjee, A., et al. 2023, ApJ, 948, 99, doi: [10.3847/1538-4357/acc65b](https://doi.org/10.3847/1538-4357/acc65b)

Zheng, Z., Coil, A. L., & Zehavi, I. 2007, ApJ, 667, 760, doi: [10.1086/521074](https://doi.org/10.1086/521074)

Zheng, Z., & Guo, H. 2016, MNRAS, 458, 4015, doi: [10.1093/mnras/stw523](https://doi.org/10.1093/mnras/stw523)

Zhou, R., Dey, B., Newman, J. A., et al. 2023, AJ, 165, 58, doi: [10.3847/1538-3881/aca5fb](https://doi.org/10.3847/1538-3881/aca5fb)

Zu, Y., & Mandelbaum, R. 2015, MNRAS, 454, 1161, doi: [10.1093/mnras/stv2062](https://doi.org/10.1093/mnras/stv2062)